journal of the mechanical behavior of biomedical materials 113 (2021) 104122

Contents lists available at ScienceDirect

Journal of the Mechanical Behavior of Biomedical Materials

journal homepage: http://www.elsevier.com/locate/jmbbm

Anatomical variations in cortical bone surface permeability: Tibia versus femur

Rakesh Kumar [a], Abhishek Kumar Tiwari [b,*], Dharmendra Tripathi [c], Russell P. Main [d], Navin Kumar [e], Praveer Sihota [e], Sonu Ambwani [f], Niti Nipun Sharma [a]

[a] Department of Mechanical Engineering, Manipal University Jaipur, Jaipur, 303007, Rajasthan, India
[b] Department of Applied Mechanics, Motilal Nehru National Institute of Technology Allahabad, Prayagraj, 211004, Uttar Pradesh, India
[c] Department of Mathematics, National Institute of Technology, Uttarakhand, 246174, India
[d] Department of Basic Medical Sciences and Weldon School of Biomedical Engineering, Purdue University, West Lafayette, IN, USA
[e] Department of Mechanical Engineering, Indian Institute of Technology Ropar, Roopnagar, 140001, Punjab, India
[f] Department of Molecular Biology and Genetic Engineering, G.B. Pant University of Agriculture and Technology, Pantnagar, 263145, Uttarakhand, India

ARTICLE INFO

Keywords:
Bone adaptation
Lacunar-canalicular system (LCS)
Permeability
Nanoindentation
Optimization

ABSTRACT

Cortical bone surfaces (periosteal and endosteal) exhibit differential (re)modelling response to mechanical loading. This poses a serious challenge in establishing an in silico model to predict site-specific new bone formation as a function of mechanical stimulus. In this regard, mechanical loading-induced fluid motion in lacunar-canalicular system (LCS) is assumed osteogenic. Micro-architectural properties, especially permeability regulate canalicular fluid motion within the bone. The knowledge of these properties is required to compute flow distribution. Along the same line, it is possible that cortical surfaces may experience differential fluid distribution due to anatomical variations in microarchitectural properties which may induce distinct new bone response at cortical surfaces. Nevertheless, these properties are not well reported for cortical surfaces in the literature. Accordingly, the present study aims to measure microarchitectural properties especially permeability at different anatomical locations (medial, lateral, anterior, and posterior) of periosteal and endosteal surfaces using nanoindentation. A standard poroelastic optimization technique was used to estimate permeability, shear modulus, and Poisson's ratio. The properties are also compared for two weight-bearing bones i.e. tibia and femur. Endosteal surface was found more permeable as compared to the periosteal surface. Tibial endosteal surface had shown greater permeability values at most of the anatomical locations as compared to femoral endosteal surface. The outcomes may be used to precisely predict site-specific osteogenesis in cortical bone as a function of canalicular flow distribution. This work may ultimately be beneficial in designing the loading parameters to stimulate desired new bone response for the prevention and the cure of bone loss.

1. Introduction

Physiological loading-induced mechanical environment regulates bone adaption (Wolff, 1893). In vivo animal loading experiments (Calbet et al., 1998; Palombaro, 2005; Srinivasan et al., 2002) have established that cyclic and low-magnitude loading on bone encourages osteogenesis i.e. new bone formation. Several in silico mathematical (Chennimalai Kumar et al., 2012; Hambli, 2010; Huiskes et al., 1992; Kumar et al., 2019; Taylor et al., 2003; Tiwari and Prasad, 2016; Van Rietbergen et al., 1993) models explained that new bone formation occurs at those locations where normal strain-magnitude or strain energy exceeds osteogenic thresholds. Nevertheless, this mathematical explanation may fail in explaining osteogenesis noticed at minimal strain sites e.g. near the neutral axis. This anomaly is indicated by several studies (Srinivasan et al., 2002; Tiwari and Prasad, 2016). In vivo and in silico studies (Burger and Klein-Nulend, 1999; Klein-Nulend et al., 2013; Pereira et al., 2015) reported that secondary components of mechanical environment such as interstitial fluid flow can also be a possible stimulus of osteogenesis. For example, Carriero et al. (2018) observed that the new bone formation at cortical surfaces (both periosteal and endosteal) occurs in regions of high fluid flow. In contrast, strain energy density fitted experimental new bone formation only at the

* Corresponding author..
E-mail address: aktiwari@mnnit.ac.in (A.K. Tiwari).

https://doi.org/10.1016/j.jmbbm.2020.104122
Received 6 July 2020; Received in revised form 10 September 2020; Accepted 28 September 2020
Available online 30 September 2020

periosteal surface. Therefore, it encourages establishing fluid flow as a stimulus of osteogenesis. Osteocyte cells embedded in bone matrix connect each other through micro-channels known as canaliculi (Prideaux et al., 2016). It is believed that mechanical loading induces fluid motion in lacunar-canalicular space which exposes the osteocyte cell body to fluid shear. This fluid shear is assumed responsible for the excitation of osteocytes for bone forming activities (Tan et al., 2007; Weinbaum et al., 1994), nevertheless, this mechanism is yet to be established.

Mathematical computation of loading-induced interstitial fluid motion requires certain microarchitectural properties such as permeability as these properties regulate the fluid motion in the lacunar-canalicular system of bone (Kumar et al., 2019). There are studies which highlighted that the two cortical envelops i.e. endosteal and periosteal surfaces respond differently to mechano-adaptation (Birkhold et al., 2017, 2016; Tiwari et al., 2018). For example, Birkhold et al. (2016) attempted to explain the mechano-responsiveness of periosteal and endosteal surfaces in murine tibia (female C57Bl/6J mice) mid-diaphyseal cross--section. They observed that the endosteal surface is more mechanoresponsive as the thickness of newly formed bone packets was greater in comparison to the periosteal surface. Moreover, this response was observed even at a lower strain magnitude. Srinivasan et al. (2010) also observed that numerical models fall short in explaining the site-specific new bone formation at the endocoritcal surface noticed at the mid-diaphyseal cross-section of murine tibia subjected to cantilever bending. Tiwari and Prasad (2016) also had limited success in their in silico studies in fitting the experimental site-specific new bone formation at the endosteal surface as a function of fluid flow. This indicates that bone adaptation may vary between different bones in the skeleton as well as different sites within the same bone. The underlying reason behind such response however is not well explored. One of the possible reasons may be that different anatomical regions and different bones experience distinct fluid motion leading to differences in mechano-responsiveness. This may be due to variations in microarchitectural properties such lacunar-canalicular permeability and vascular porosity in anatomical regions. Several studies have reported that lacunar-canalicular permeability (Gururaja et al., 2005; Smit et al., 2002; Wang, 2018; Weinbaum et al., 1994) of cortical bone typically vary in a range of 10^{-22}-10^{-19} m^2. Rodriguez-Florez et al. (2014) experimentally measured lacunar-canalicular permeability at the mid-diaphyseal cortex of a C57Bl/6J mouse tibia using nanoindentation and standard poroelastic optimization technique. They observed permeability lies in the range of 10^{-24} m^2. Benalla et al. (2012) observed that lacunar-canalicular system (LCS) permeability of human osteon lies in the range of 10^{-17}-10^{-25} m^2. Rodriguez-Florez et al. (2014) estimated age-related change in permeability of C57BL/6 mouse tibia using nanoindentation method proposed by Oyen (2008). Canalicular permeability is observed in a range of 5×10^{-25} to 10^{-21} m^2. They have suggested that lacunar-canalicular intrinsic permeability decreases from 2 to 7 months and then no significant change occurs from 2 to 7 months. The literature suggests that canalicular permeability of cortical bone ranges from 10^{-25} to 10^{-18} m^2.

It is worth mentioning that mechanical properties of murine, bovine, canine, and porcine bone tissues are widely characterized using various experimental techniques such as nanoindentation (Casanova et al., 2017; Isaksson et al., 2010), Dynamic Measurement Analysis (Kumar et al., 2017) and Computer Tomography (Jast and Jasiuk, 2013) at micro and macro scales. The literature suggests that mechanical properties of bone vary with bone type, anatomical locations, and directions within the same bone tissue (Kotha et al., 1998). Nevertheless, there are very few studies (Berteau et al., 2016; Cardoso et al., 2013) which characterized the poro-mechanical properties with respect to bone type and anatomical locations. There is hardly any known study that had comprehensively analyzed and compared the poromechanical properties such as permeability of the two critical weight-bearing long bones i.e. tibia and femur. Moreover, the variation of these properties has not been studied concerning the anatomical regions of the cortex i.e., anterior, posterior, medial, and lateral regions, and the cortical bone envelops (periosteal and endosteal). To fill this gap, the present work aims to characterize the poromechanical properties such as permeability and shear modulus of the cortical surfaces i.e. periosteal and endosteal surfaces. To serve this purpose, the mid-shaft cortex of rat tibia and femur are chosen. A standard nanoindentation technique (Oyen, 2008) is used to characterize the permeability of the two surfaces. Poromechanical properties of rat tibia and femur are also compared. These properties are estimated across different anatomical locations (anterior, posterior, medial, and lateral) of the cortex across periosteal and endosteal envelopes. The outcomes will improve the understanding on the reason behind the distinct mechano-responsiveness of the two surfaces in different anatomical regions. This work may be useful in the precise estimation of loading-induced fluid flow in the cortical bone. The outcomes may be extended to develop a robust computer model for the prediction of in vivo new bone formation.

2. Materials and methods

2.1. Preparation of samples

Thirty Wistar rats of 7 months (skeletally mature) were used in the study. The animals were humanely handled and were sacrificed as per the guidelines of Institutional Animal Ethics committee of G.B. Pant University of Agriculture and Technology, Pantnagar, India. Rats were euthanized and knee joints along with tibial and femoral bones were separated at animal house facility at G.B. Pant University of Agriculture and Technology, Pantnagar, Uttarakhand, India. Animals were sacrificed as per the protocol approved by Institutional ethics committee of G.B. Pant University of Agriculture and Technology, India. Distal femoral end and proximal tibia end were disconnected at knee joint using surgical procedures. Tissues surrounding the femur and tibia were removed followed by a soft water jet and ultrasonic bath. To avoid dehydration, bone samples were immediately soaked in phosphate buffer saline (PBS) and then wrapped in gauze. The samples were then preserved at −20 °C. A standard procedure reported in the literature was followed to preserve the mechanical properties of bone tissue (Oyen, 2008; Rodriguez-Florez et al., 2014). Bone tissues were thawed at 4–5 °C before segmentation. Length of tibia and femur bones was measured. Bones were sliced in 3–4 thick sections in mid-diaphyseal region at half-length of the bone (Fig. 1(a)). IsoMet™ Buehler low-speed saw was used for slicing of cortical bone sections. Tissue sections were dried and then embedded in epoxy resin (EPOTHIN, Buehler, Lake Bluff, Illinois, USA) using hardner. It is observed that epoxy-resin mixture does not influence the mechanical properties of bone tissue (Hoffler et al., 2005) much. Thus, the samples were immersed in the mixture keeping the indented surface i.e. tibia or femur cross-section covered and intact, and the mixture was also allowed to be cooled for 15 min to avoid infiltration of resin into pores. EcoMet™ 250 (Buehler) was used to polish the embedded surface of cortical sections using different grades of carbide papers (P600, P1000, P1200, and P2400) and diamond slurries (9, 3, 1, 0.25 and 0.05 μm). A constant water jet of ionized water was also maintained to avoid dehydration. Polishing was done for 2–3 min under deionized water. Constant pressure was applied on the samples to attain a superior finish for nanoindentation. Surface roughness was also measured before performing the indentation.

2.2. Nanoindentation

Nanoindentation method proposed by Oliver and Pharr (2004) is a most commonly used method to determine the mechanical properties of materials. Nanoindentation method was used here in the present study to estimate another important poromechanical property i.e. permeability. Bone samples were hydrated in distal water bath at room temperature before indentation. Triboindenter 950 (Hysitron Inc.

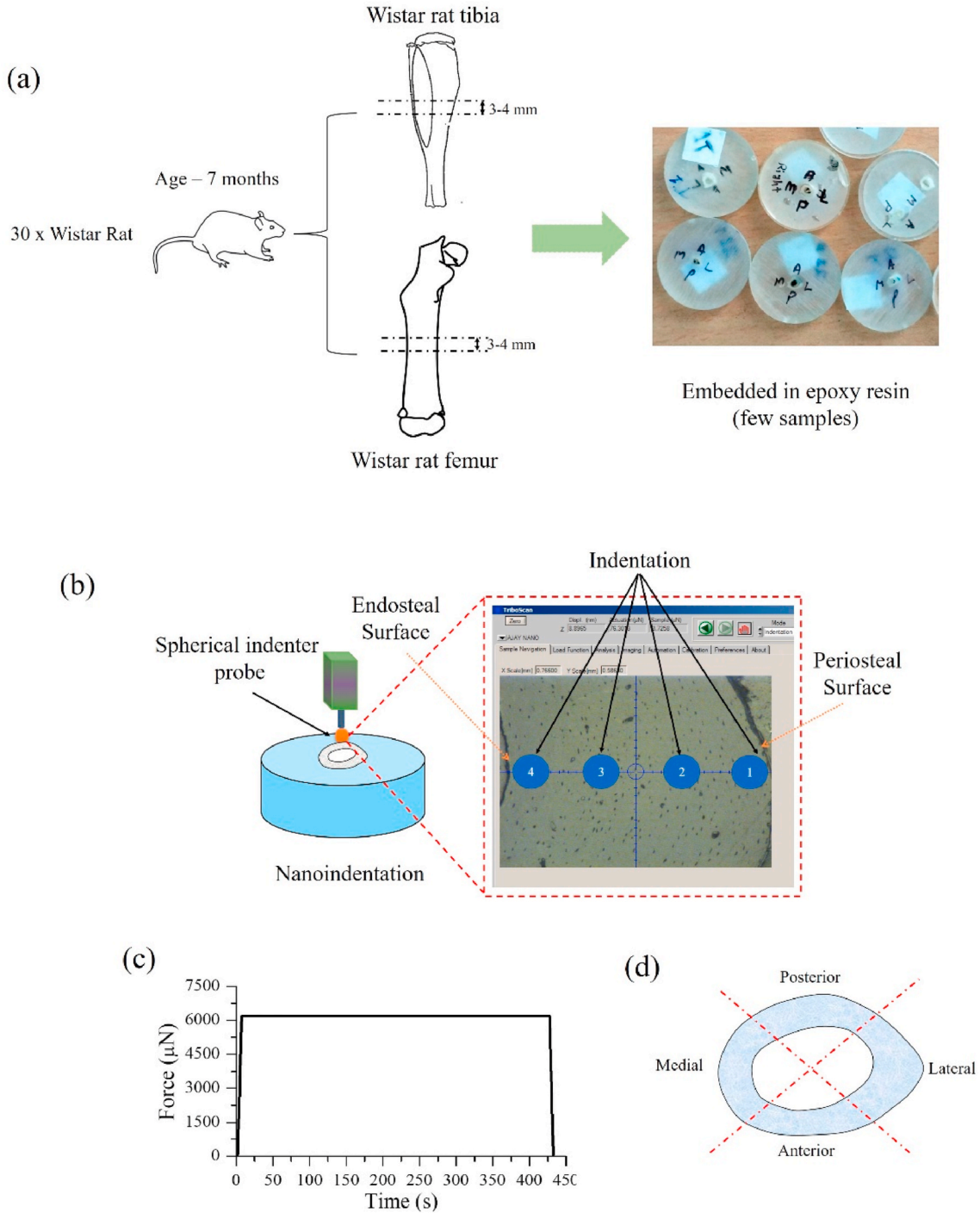

Fig. 1. Sample preparation and nanoindentation procedure: (a) mid-diaphyseal cross-section of femoral and tibial cortex embedded in epoxy resin; (b) nanoindentation scheme, (c) trapezoidal loading waveform, and (d) mid-cortex anatomical positioning in anterior, posterior, medial and lateral sectors.

Minneapolis, USA) was used to perform nanoindentation in load-control mode with a spherical indenter of diameter 200μm. A trapezoidal loading waveform with rising time of 10 s with peak load of 6000μN and dwell time of 410 s was selected for indentation (Rodriguez-Florez et al., 2014) (Fig. 1(c)). Tibiae and femur bone mid-diaphyseal cross-sections were divided into four anatomical regions namely anterior, posterior, medial, and lateral (Fig. 1(d)). Periosteal and endosteal surfaces of the cortex were identified using a microscope attached with nanoindentation setup. Four indents were radially performed within each anatomical region. The cortex thickness of bone cross-sections were measured across the anatomical locations with the help of Tribo-nano-indenter. Indent 1 was performed at the outer periphery near the periosteal surface. Indentation location was selected slightly away from the resin-bone interface to minimize the effect on fluid-pressure response. Indent 4 was performed near the inner boundary i.e. endosteal surface. Indents 2 and 3 were performed at 25% of cortical thickness from indents 1 and 4, respectively, as shown in Fig. 1 (b). In addition, the same loading waveform was applied in all the regions. Experimental data i.e. $P - h - t$ shown in Figure (2) and (3) were imported in MATLAB (MathWorks, Natick, MA, USA). Load-displacement curve with large impractical variations are discarded since indenter may sometimes fall into pores resulting in unphysical

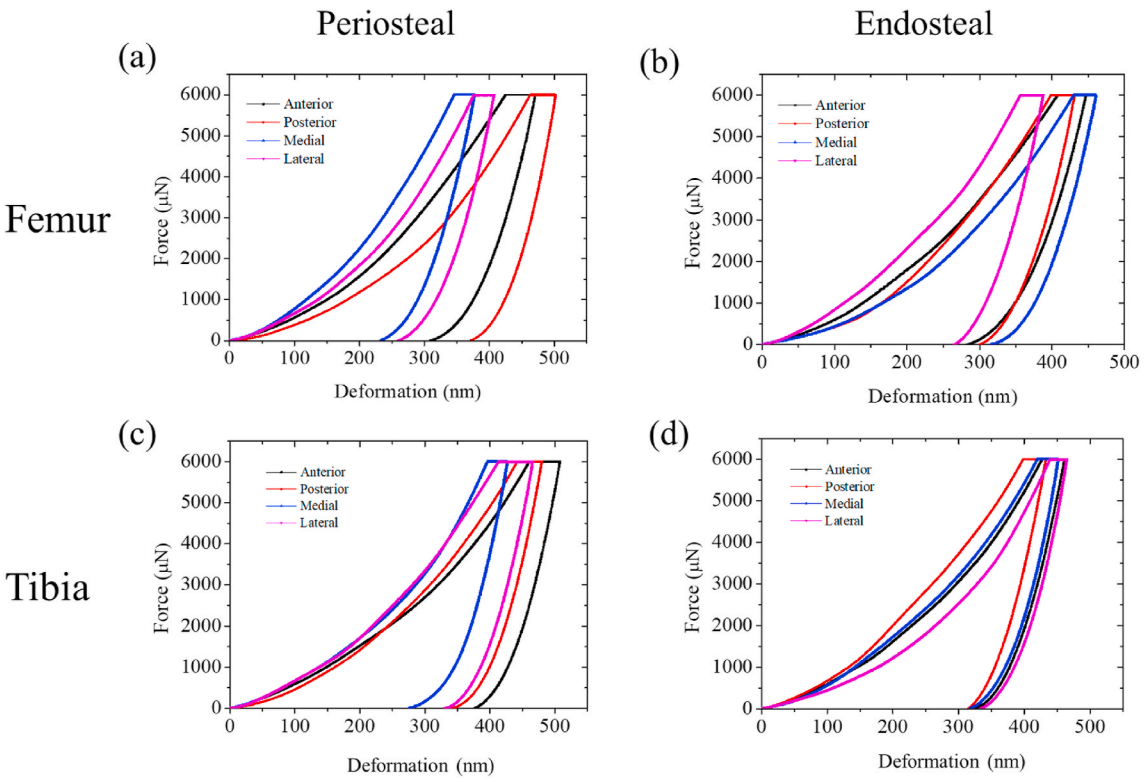

Fig. 2. Force-deformation $(p-h)$ curve obtained from indentation of Wistar rat femur ((a) and (b)), tibia ((c) and (d)) cross-section at periosteal and endosteal surface, respectively.

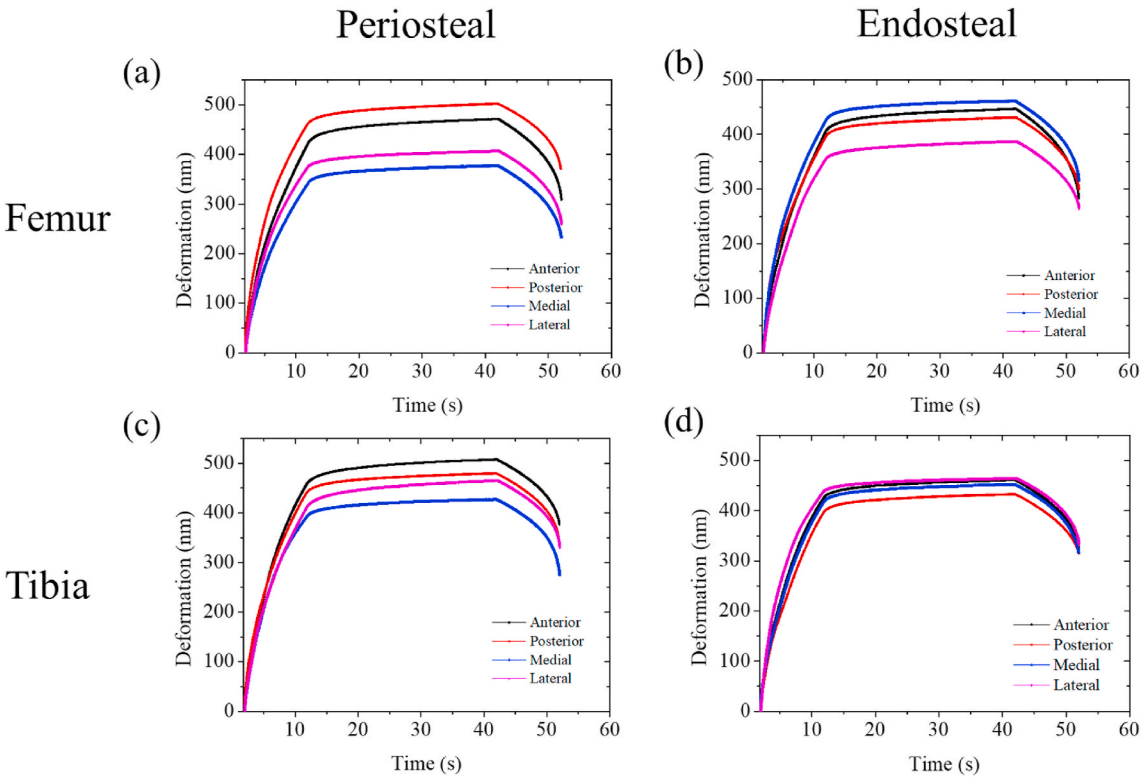

Fig. 3. Deformation-time $(h-t)$ curve obtained for femur ((a) and (b)), and tibia ((c) and (d)) tibia cross-section at periosteal and endosteal surface, respectively.

data. A total 52 (26 (rat samples) × 2 (number of indentations)) $p-h$ curves are averaged to obtain the mean curve for cortical surface in each anatomical region. The data from four samples were discarded due to improper indentation.

2.3. Poroelastic analysis

The poroelastic method of permeability measurement involves the measurement of creep response of porous-hydrated biological material as proposed by Oyen (2008) and Galli and Oyen (2009). The indenter pushes the water out of the material during contact. This results in pore-pressure development which supports the applied load partially. Pore-Pressure drops as soon as fluid leaves the local space. Thus, load-deformation exhibit time-dependent response which was recorded as *P-h-t* curve. The poroelastic response is usually characterized using five parameters (Rodriguez-Florez et al., 2014) namely shear modulus (G), drained Poisson's ratio (ν), undrained Poisson's ratio (ν_u), and Biot-Willi's effective stress coefficient ($\alpha = 1 - \frac{K}{K_s}$, in which K is the bulk modulus of the drained bone tissue and K_s of solid bone material) and intrinsic permeability (k). Porous material is assumed linearly elastic, homogeneous, and isotropic. The estimation of intrinsic permeability (k) which characterizes the flow through porous bone material has been taken as the objective of the present study.

Galli and Oyen (2009) proposed an algorithm to estimate poroelastic parameters based on a master curve library developed from nano-indentation experiments and finite element analysis on different materials. This method non-dimensionalizes the indentation displacement as:

$$h^* = \frac{h(t) - h_o(t)}{h_\infty(t) - h_o(t)} \tag{1}$$

where $h(t)$ is indentation depth at any arbitrary time t; $h_o(t)$ is indentation depth measured at instant t under step loading conditions with undrained conditions and $h_\infty(t)$ is measured at $t = \infty$ when the pore-pressure vanishes. $h_o(t)$ and $h_\infty(t)$ can be defined as (Rodriguez-Florez et al., 2013):

$$h_o(t) = \left(\frac{3P(t)(1-\nu_u)}{8GR^{0.5}}\right)^{2/3} \tag{2}$$

$$h_\infty(t) = \left(\frac{3P(t)(1-\nu)}{8GR^{0.5}}\right)^{2/3} \tag{3}$$

where *P(t)* represents indentation load and R is the indenter tip radius. The time is also normalized using the following equation:

$$t^* = \sqrt{\frac{ct}{Rh(t)}} \tag{4}$$

where diffusivity coefficient c is calculated as:

$$\left(= \frac{2kG(1-\nu)(\nu_u - \nu)}{\alpha^2(1-2\nu)^2(1-\nu_u)}\right)$$

An optimization algorithm with a sub-space trust region method of minimization is used to estimate the unknown poroelastic parameters (Fig. 4). The method allows the computation of three parameters while the other two parameters are kept fixed (Galli and Oyen, 2009). In the present work G, ν and k are estimated while the other two poroelastic parameters i.e. α and ν_u are set to 1 and 0.5, respectively (Galli and Oyen, 2009). A vector $x(G, k, \nu)$ is designed with three unknown parameters to be identified using non-linear least-squares optimization routine. Experimental displacement-time curve is used as input which is interpolated on a grid of m equally spaced points (h_1, t_1).....(h_m, t_m). Two step optimization is used, where, the first step occurs in the normalized domain (x^*, h^* *and* t^*) in which the normalized curves were fitted to the master curves. The second optimization routine attempts to verify the solution obtained in the first step by fitting the dimensional

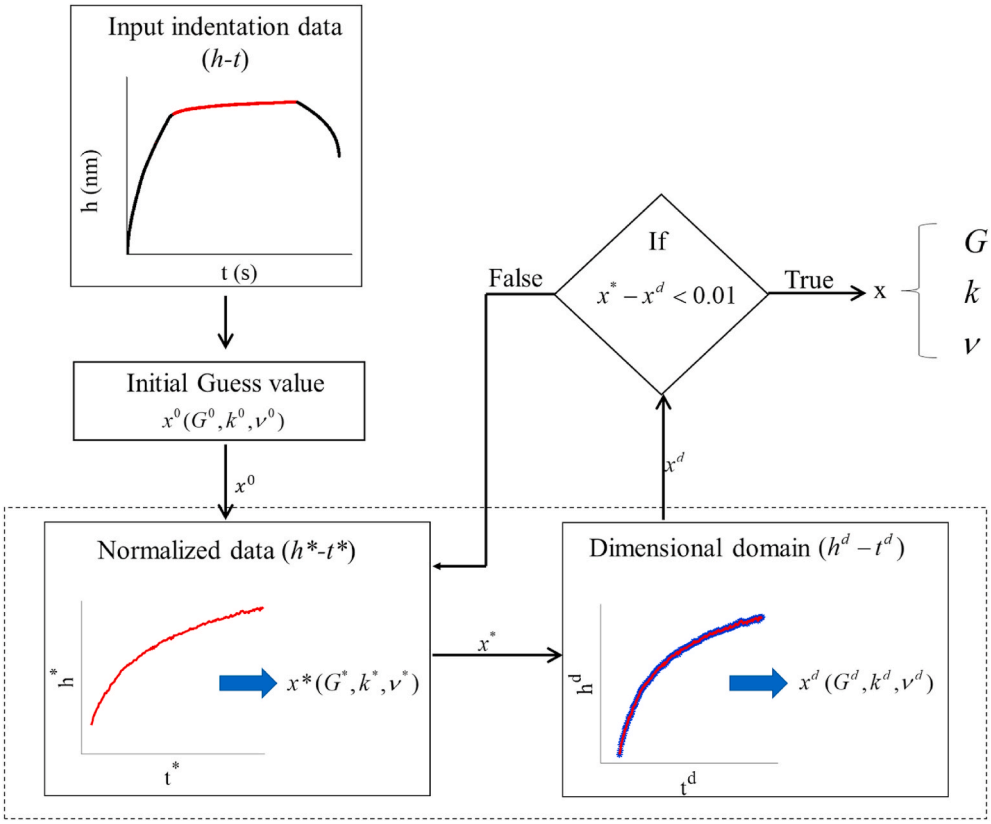

Fig. 4. Algorithm used to calculate poromechanical parameters based on Oyen (2008).

domain. This means that the solution (x^* (G^*, k^*, ν^*)) obtained from normalized domain with best fit is supplied in dimensional domain and the new dimensional solution (x^d (G^d,k^d,ν^d)) is computed. Curve fittings were done with non-linear least square optimization using custom written code in MATLAB (MathWorks, Natick, MA, USA). Convergence was achieved when the difference among the parameters identified in normalized and dimensional domain was found negligible i.e., $(x^* - x^d) < 0.01$.

2.4. Statistical analysis

Statistical analysis is carried out to evaluate the accuracy of multiple measurements of a micro-architectural property performed during experiments. Permeability, shear modulus, and Poisson's ratio at the different anatomical locations of tibial and femoral bone cross-section were estimated. Two statistical tests namely t-test and z-test were carried out. A t-test was used to examine whether the poromechanical properties obtained at two anatomical positions vary statistically from each other or not. A significance level of 0.05 is considered. The hypothesis result (**h**) equals to zero in the t-test signifies that it does not reject the null hypothesis at the default meaning level of 5 percent. Z-test is also used to assess whether mean poromechanical properties estimated at two anatomical locations are significantly different or not. Hypothesis value (h) is equal to zero and $Z_{val} < 0.001$ signifies that z-test does not reject the null hypothesis at the significance level of 5 percent. All statistical analysis was performed using MATLAB (MathWorks, Natick, MA, USA).

3. Results

3.1. Shear modulus

This section presents the comparison of shear modulus distribution at different anatomical locations (medial, lateral, anterior, and posterior) of tibia and femur bone. Statistical results indicate that shear modulus evaluated at femur and tibia cross-sections are not significantly different, however, it varies across cortical envelops as shown in Tables 1 and 2. It is noticed that the endosteal surface at femur cross-section has higher shear modulus in anterior and posterior regions, whereas, the periosteal surface has a higher modulus in medial and lateral regions (Figs. 5 and 6). The endosteal surface of tibia exhibit higher shear modulus as compared to the periosteal surface in all anatomical regions except the lateral region (Fig. 6). The magnitude of shear modulus lies within the range of 500–700 MPa which also aligns with the findings of Rodriguez-Florez et al. (2014).

3.2. Lacunar canalicular permeability

Lacunar-canalicular permeability of Wistar rat femora and tibiae were measured at a mid-diaphyseal cross-section at different anatomical locations (medial, lateral, anterior, and posterior) as shown in Fig. 7. Mean values of permeability along with standard deviations were plotted at periosteal and endosteal surfaces in anatomical regions. The endosteal surface was found more permeable as compared to the periosteal surface across all the anatomical regions in both femur and tibia. The endosteal surface of tibia has higher permeability as compared to endosteal region of femur (Fig. 8). The calculated permeability values are observed in the range of 5×10^{-24} m^2 to 7×10^{-24} m^2. Lacunar permeability of femur and tibia are also compared. The tibial cortex has greater permeability in the endosteal region as compared to the femoral cortex. A lower permeability is observed in anterior and lateral sectors in comparison to femur cortical bone at the periosteal surface. The same can be noticed in Fig. 8.

3.3. Poisson's ratio

Poisson's ratio of Wistar rat femora and tibia were measured at mid-diaphyseal cross-section at different anatomical locations (medial, lateral, anterior, and posterior). The results demonstrate that Poisson's ratio does not change significantly with anatomical locations. The values lie within the range of 0.33–0.37. Rodriguez-Florez et al. (2014) also reported similar Poisson's ration for B6 mice. No statistical difference is observed in anatomical distribution of Poisson's ratio.

4. Discussion

Nanoindentation is used to compute the poromechanical properties of cortical bone envelopes. Anatomical variation of these properties is also studied which is the essence of the present study. The endosteal surface is found more permeable as compared to the periosteal surface in the tibia as well as femur bone. Periosteal surface permeability value lies in between 3×10^{-24} to 4.5×10^{-24} m^2, whereas, the endosteal surface permeability lies in between 3.8×10^{-24} to 6.5×10^{-24} m^2 (Fig. 8). These values are also found in the range reported in previous experiments (Beno et al., 2006; Cardoso et al., 2013; Rodriguez-Florez et al., 2014). There is hardly any study that indicates the anatomical variation in poromechanical properties of long bones and across their cortex. The present experimental study highlights that shear modulus varies with anatomical sites namely anterior, posterior, medial, and lateral regions of the cortex. Endosteal surface exhibits higher shear modulus in anterior, posterior, and medial regions. The drained Poisson's ratio computed in this study are also found within the range reported in Rodriguez-Florez et al. (2014). Nevertheless, these values also depend on the way experiment is conducted (Rodriguez-Florez et al., 2013). Cellular structures inside the lacunae may change when bone cross-section is embedded in the epoxy resin, and it is observed that permeability may decrease when cellular architecture is accounted for in the analysis (Anderson et al., 2008; Pereira and Shefelbine, 2014). All the values are assumed to be influenced by same amount due to similar testing protocol.

Poroelastic material is characterized using five constitutive parameters. Out of these parameters, only three can be obtained from nanoindentation method with spherical indenter (Rodriguez-Florez et al., 2014, 2013). Oyen (2008) also measured equine bone permeability

Table 1
T-test performed between anatomical location of femur and tibia at periosteal and endosteal surface.

Bone Tissue	Cortical Surface	Anatomical Locations	Permeability (k)		Shear Modulus (G)		Poisson's ratio (ν)	
			h	p	h	p	h	p
Femur	Periosteal	Lateral vs. Medial	0	0.88	0	0.965	0	0.3021
		Anterior vs. Posterior	0	0.83	0	0.528	0	0.8407
	Endosteal	Lateral vs. Medial	0	0.37	0	0.866	0	0.524
		Anterior vs. Posterior	0	0.67	0	0.671	0	0.6236
Tibia	Periosteal	Lateral vs. Medial	0	0.36	0	0.21	0	0.454
		Anterior vs. Posterior	0	0.61	0	0.45	0	0.511
	Endosteal	Lateral vs. Medial	0	0.72	0	0.77	0	0.82
		Anterior vs. Posterior	0	0.75	0	0.81	0	0.84

Table 2
Z-test performed at different anatomical location of Femur and Tibia bone.

Z-Test											
Bone Tissue	Cortical Surface	Anatomical Locations	Permeability (k)			Shear Modulus (G)			Poisson's ratio (ν)		
			h	p	Z_{val}	h	p	Z_{val}	h	p	Z_{val}
Femur	Periosteal	Anterior	0	1	3.04×10^{-4}	0	1	3.36×10^{-10}	0	1	7.12×10^{-13}
		Lateral	0	1	0.0099	0	1	8.04×10^{-10}	0	1	4.78×10^{-09}
		Medial	0	1	2.41×10^{-4}	0	1	4.66×10^{-10}	0	1	5.57×10^{-08}
		Posterior	0	1	0.0011	0	1	1.17×10^{-09}	0	1	8.80×10^{-13}
	Endosteal	Anterior	0	1	5.11×10^{-5}	0	1	3.78×10^{-8}	0	1	2.89×10^{-14}
		Lateral	0	1	1.15×10^{-5}	0	1	2.75×10^{-8}	0	1	3.19×10^{-13}
		Medial	0	1	2.88×10^{-6}	0	1	5.68×10^{-7}	0	1	8.29×10^{-14}
		Posterior	0	1	7.05×10^{-4}	0	1	6.54×10^{-8}	0	1	6.71×10^{-14}
Tibia	Periosteal	Anterior	0	1	7.46×10^{-3}	0	1	4.98×10^{-9}	0	1	3.16×10^{-13}
		Lateral	0	1	2.83×10^{-3}	0	1	3.79×10^{-9}	0	1	4.82×10^{-13}
		Medial	0	1	3.97×10^{-3}	0	1	8.94×10^{-9}	0	1	3.68×10^{-13}
		Posterior	0	1	6.18×10^{-4}	0	1	2.61×10^{-9}	0	1	6.81×10^{-13}
	Endosteal	Anterior	0	1	3.64×10^{-4}	0	1	1.62×10^{-10}	0	1	6.45×10^{-14}
		Lateral	0	1	4.82×10^{-4}	0	1	2.63×10^{-10}	0	1	5.36×10^{-14}
		Medial	0	1	7.52×10^{-4}	0	1	3.72×10^{-10}	0	1	4.73×10^{-14}
		Posterior	0	1	5.23×10^{-4}	0	1	2.19×10^{-10}	0	1	2.25×10^{-14}

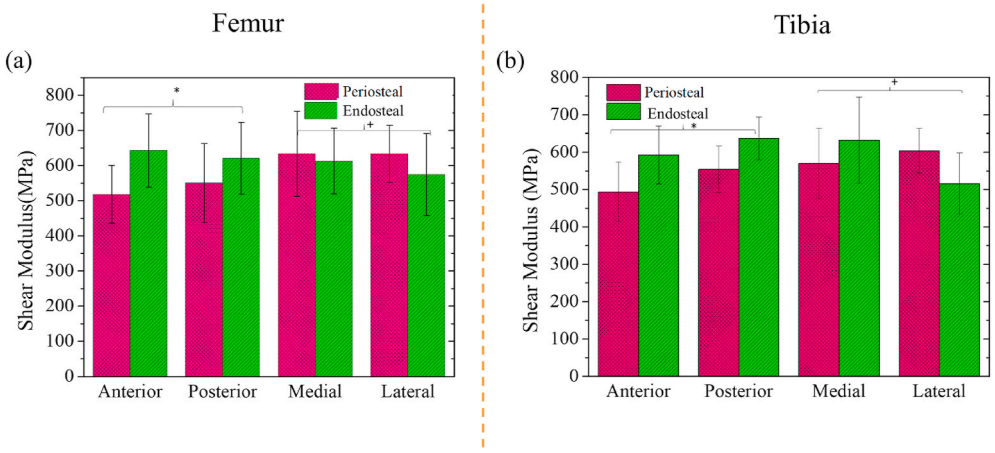

Fig. 5. Mean and standard deviations of shear modulus of: (a) Femur and (b) Tibia in different anatomical regions.

$(= 10^{-24}\ \mathrm{m}^2)$ using a spherical indenter while keeping Biot-Willis effective stress coefficient α as 1 and undrained Poisson's ratio (ν_u) as 0.5. The effective stress coefficient value lies between α [0, 1]. It depends upon the bone elastic property, osteonal structure, and age. For non-osteonal bone, such as in murine bone, the stress coefficient can be assumed as $\alpha = 1$ (Shefelbine and Carter, 2004), which we have preferred in this work, as this value provides a good estimation of permeability values for non-osteonal bone.

The poroelastic framework used in the present study assumes that material has linear isotropic poroelastic behavior. It is difficult to investigate more complicated mechanical behavior due to anisotropy in bone microstructure. The present study measures poroelastic properties in a fixed orientation, nevertheless, quantitative and qualitative differences may exist in other orientation. The measured poromechanical response depends on the physical structure which may affect the fluid flow differently in other tissue orientations. Axial experiments may not be suitable for characterization of an anisotropic and inhomogeneous composite material such as bone. The combination of assumptions of isotropy, fluid incompressibility, and a purely poroelastic flow mechanism in the analysis provides a quantitative evaluation of hydraulic and intrinsic permeability which are nothing but "effective" values under the defined assumptions. Future work may look into the measurement of anisotropic permeability of the cortical bone tissue.

Those indentation data were discarded which exhibited a large/impractical variation in the load-displacement curve. It is expected that such data will provide impractical material properties. Ramezanzadehkoldeh and Skallerud (2017) also mentioned that load-displacement parameters shall be determined from cavity-free responses. These data were excluded in the best possible way during poromechanical analysis. There are studies where indenter probes of different sizes are used to identify both lacunar-canalicular and vascular permeability. Rodriguez-Florez et al. (2014) noticed that permeability value also increases with an increase in the contact size of the indenter. There is no correlation between the indenter contact size and shear modulus, however, it depends upon the state (hydrated/de-hydrated) of the bone sample. Previous studies (Rodriguez-Florez et al., 2014, 2013) have shown that shear modulus decreases when spherical indenter is used in place of Bercovich indenter (sharp indenter). We have used 200 μm tip indenter in the present study to more closely capture the permeability data.

Previous studies (Birkhold et al., 2016; Tiwari et al., 2018) on bone adaptation have shown that the periosteal and endosteal surface of cortical bone has a different remodelling response. In silico model fails

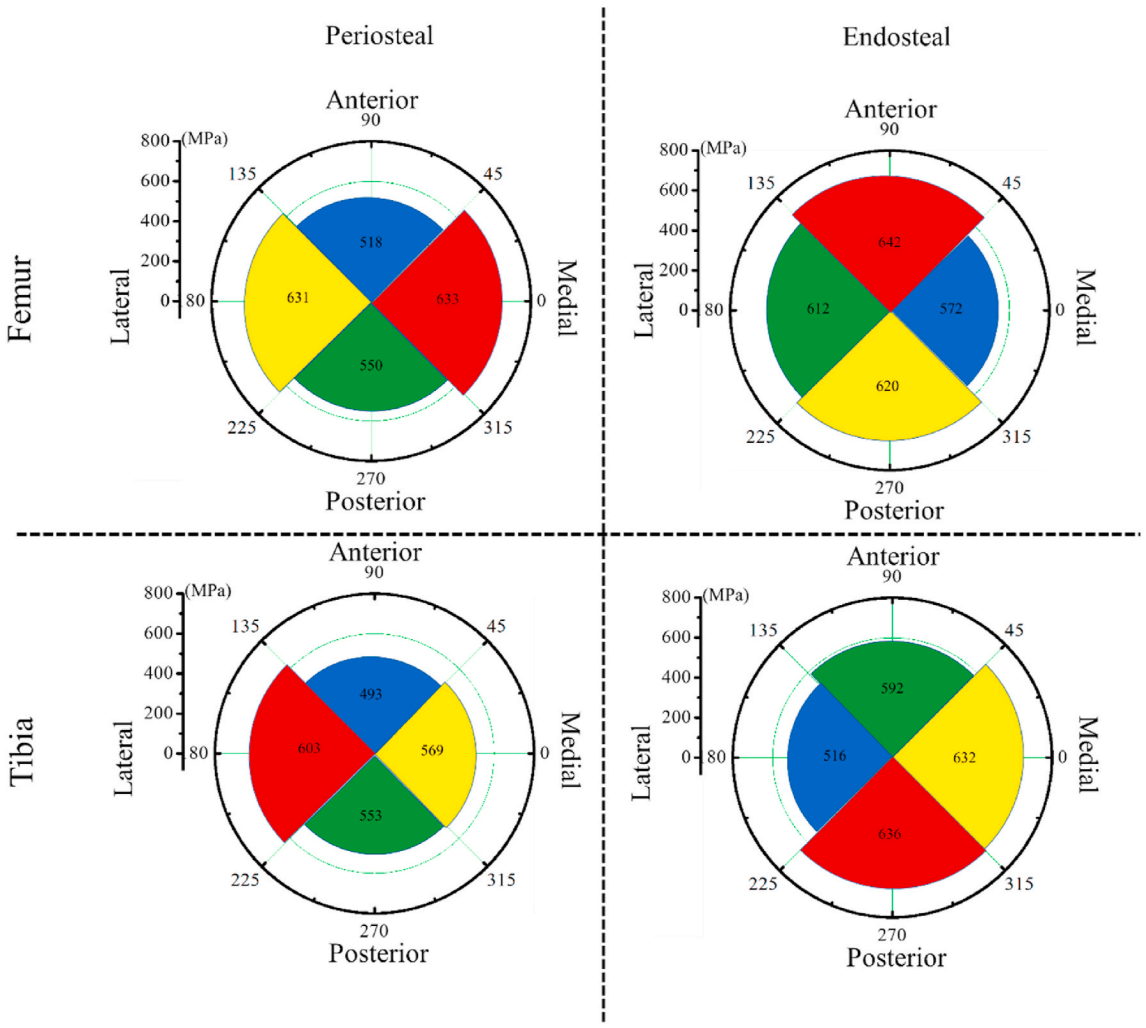

Fig. 6. Distribution of shear modulus across periosteal and endosteal surface in different anatomical regions of tibia and femur.

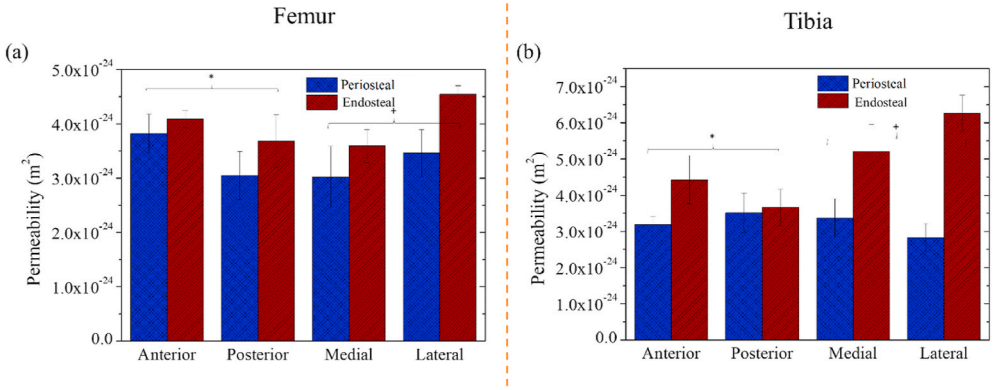

Fig. 7. Mean and standard deviations of permeability of: (a) Femur and (b) Tibia bone in different anatomical regions.

to produce osteogenesis especially at the endosteal region. One such explanation could be the assumption of the same material properties such as permeability, Poisson's ratio, and shear modulus at both the region. Generally, bone adaption occurs at the site of maximal strain distribution and the endosteal surface shows higher mechano-responsiveness as compared to the periosteal surface. Pereira and Shefelbine (2014) reported that pore pressure and fluid motion highly depend on lacunar-canalicular permeability. Bone adaptation response also varies between different bones and even with different anatomical sites of the same bone. The difference in permeability and altered fluid motion due to variation in the microarchitectural environment may be a possible explanation of the variation of differential mechano-responsiveness of anatomical sites in bone. Therefore, this work presents a fundamental estimation of cortical bone poromechanical properties at different anatomical sites.

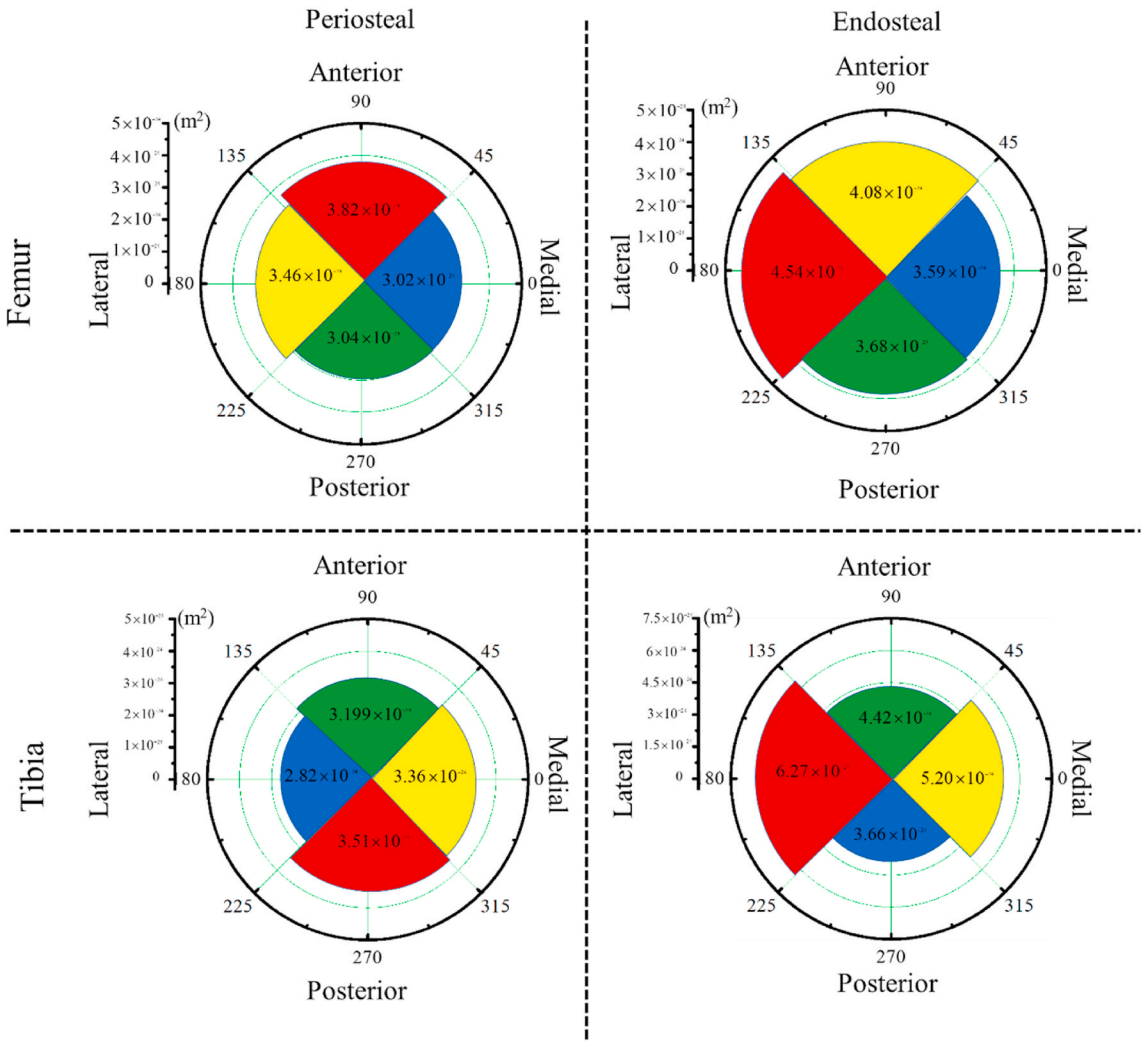

Fig. 8. Distribution of permeability across periosteal and endosteal surface at different anatomical locations of tibia and femur.

5. Conclusions

The present study estimates poromechanical properties of cortical bone surfaces in different anatomical regions of two different long bones. It is observed that the endosteal surface is more permeable as compared to the periosteal surface in all the anatomical sectors of tibia and femur. The outcomes of the study suggest that poromechanical properties changes with location and regions at periosteal and endosteal surfaces. The findings of the study may be useful in the precise estimation of mechanical environment required for modelling and remodelling activities. This understanding may be beneficial to improve biomechanical interventions to treat bone loss. These findings may also be useful in characterizing the mechanical environment and understanding the bone remodelling around bone-implant interface.

CRediT authorship contribution statement

Rakesh Kumar: Investigation, Conceptualization, Formal analysis, Writing - original draft. **Abhishek Kumar Tiwari:** Supervision, Conceptualization, Investigation, Methodology, Formal analysis, Writing - review & editing, Visualization. **Dharmendra Tripathi:** Supervision, Methodology, Writing - review & editing. **Russell P. Main:** Writing - review & editing. **Navin Kumar:** Resources, Investigation. **Praveer Sihota:** Methodology, Investigation. **Sonu Ambwani:** Resources, Methodology. **Niti Nipun Sharma:** Formal analysis, Supervision.

Declaration of competing interest

The authors declare that they have no known competing financial interests or personal relationships that could have appeared to influence the work reported in this paper.

Acknowledgement

The authors acknowledge the experimental facility of IIT Ropar and G.B. Pant University of Agriculture and Technology, Pantnagar.

References

Anderson, E.J., Kreuzer, S.M., Small, O., Knothe Tate, M.L., 2008. Pairing computational and scaled physical models to determine permeability as a measure of cellular communication in micro-and nano-scale pericellular spaces. Microfluid. Nanofluidics 4, 193–204.

Benalla, M., Cardoso, L., Cowin, S., 2012. Analytical basis for the determination of the lacunar–canalicular permeability of bone using cyclic loading. Biomech. Model. Mechanobiol. 11, 767–780.

Beno, T., Yoon, Y.-J., Cowin, S.C., Fritton, S.P., 2006. Estimation of bone permeability using accurate microstructural measurements. J. Biomech. 39, 2378–2387.

Berteau, J.-P., Oyen, M., Shefelbine, S., 2016. Permeability and shear modulus of articular cartilage in growing mice. Biomech. Model. Mechanobiol. 15, 205–212.

Birkhold, A.I., Razi, H., Duda, G.N., Checa, S., Willie, B.M., 2017. Tomography-based quantification of regional differences in cortical bone surface remodeling and

mechano-response. Calcif. Tissue Int. 100, 255–270. https://doi.org/10.1007/s00223-016-0217-4.
Birkhold, A.I., Razi, H., Duda, G.N., Weinkamer, R., Checa, S., Willie, B.M., 2016. The periosteal bone surface is less mechano-responsive than the endocortical. Sci. Rep. 6, 23480.
Burger, E.H., Klein-Nulend, J., 1999. Mechanotransduction in bone—role of the lacuno-canalicular network. Faseb. J. 13, S101–S112.
Calbet, J., Moysi, J., Dorado, C., Rodriguez, L., 1998. Bone mineral content and density in professional tennis players. Calcif. Tissue Int. 62, 491–496.
Cardoso, L., Fritton, S.P., Gailani, G., Benalla, M., Cowin, S.C., 2013. Advances in assessment of bone porosity, permeability and interstitial fluid flow. J. Biomech. 46, 253–265.
Carriero, A., Pereira, A., Wilson, A., Castagno, S., Javaheri, B., Pitsillides, A., Marenzana, M., Shefelbine, S., 2018. Spatial relationship between bone formation and mechanical stimulus within cortical bone: combining 3D fluorochrome mapping and poroelastic finite element modelling. BoneKEy Rep. 8, 72–80.
Casanova, M., Balmelli, A., Carnelli, D., Courty, D., Schneider, P., Müller, R., 2017. Nanoindentation analysis of the micromechanical anisotropy in mouse cortical bone. R. Soc. Open Sci. 4, 160971.
Chennimalai Kumar, N., Dantzig, J.A., Jasiuk, I.M., 2012. Modeling of cortical bone adaptation in a rat ulna: effect of frequency. Bone 50, 792–797. https://doi.org/10.1016/j.bone.2011.12.008.
Galli, M., Oyen, M., 2009. Fast identification of poroelastic parameters from indentation tests. Cmes-Comput. Model. Eng. Sci. 48, 241–269.
Gururaja, S., Kim, H., Swan, C., Brand, R., Lakes, R., 2005. Modeling deformation-induced fluid flow in cortical bone's canalicular–lacunar system. Ann. Biomed. Eng. 33, 7–25.
Hambli, R., 2010. Application of neural networks and finite element computation for multiscale simulation of bone remodeling. J. Biomech. Eng. 132, 114502. https://doi.org/10.1115/1.4002536.
Hoffler, C.E., Guo, X.E., Zysset, P.K., Goldstein, S.A., 2005. An Application of Nanoindentation Technique to Measure Bone Tissue Lamellae Properties.
Huiskes, R., Weinans, H., Van Rietbergen, B., 1992. The relationship between stress shielding and bone resorption around total hip stems and the effects of flexible materials. Clin. Orthop. 124–134.
Isaksson, H., Nagao, S., Ma\Lkiewicz, M., Julkunen, P., Nowak, R., Jurvelin, J.S., 2010. Precision of nanoindentation protocols for measurement of viscoelasticity in cortical and trabecular bone. J. Biomech. 43, 2410–2417.
Jast, J., Jasiuk, I., 2013. Age-related changes in the 3D hierarchical structure of rat tibia cortical bone characterized by high-resolution micro-CT. J. Appl. Physiol. 114, 923–933.
Klein-Nulend, J., Bakker, A.D., Bacabac, R.G., Vatsa, A., Weinbaum, S., 2013. Mechanosensation and transduction in osteocytes. Bone 54, 182–190.
Kotha, S., Walsh, W., Pan, Y., Guzelsu, N., 1998. Varying the mechanical properties of bone tissue by changing the amount of its structurally effective bone mineral content. Bio Med. Mater. Eng. 8, 321–334.
Kumar, R., Tiwari, A.K., Sihota, P., Tripathi, D., Kumar, N., Ahmad, A., Ambwani, S., 2017. Investigation on viscoelastic properties of cortical surfaces using dynamic mechanical analysis. In: International Conference on Advances in Thermal Systems, Materials and Design Engineering (ATSMDE2017).
Kumar, R., Tiwari, A.K., Tripathi, D., Shrivas, N.V., Nizam, F., 2019. Canalicular fluid flow induced by loading waveforms: a comparative analysis. J. Theor. Biol. 471, 59–73.
Oliver, W.C., Pharr, G.M., 2004. Measurement of hardness and elastic modulus by instrumented indentation: advances in understanding and refinements to methodology. J. Mater. Res. 19, 3–20.
Oyen, M.L., 2008. Poroelastic nanoindentation responses of hydrated bone. J. Mater. Res. 23, 1307–1314.
Palombaro, K.M., 2005. Effects of walking-only interventions on bone mineral density at various skeletal sites: a meta-analysis. J. Geriatr. Phys. Ther. 28, 102–107.
Pereira, A.F., Javaheri, B., Pitsillides, A., Shefelbine, S., 2015. Predicting cortical bone adaptation to axial loading in the mouse tibia. J. R. Soc. Interface 12, 20150590.
Pereira, A.F., Shefelbine, S.J., 2014. The influence of load repetition in bone mechanotransduction using poroelastic finite-element models: the impact of permeability. Biomech. Model. Mechanobiol. 13, 215–225.
Prideaux, M., Findlay, D.M., Atkins, G.J., 2016. Osteocytes: the master cells in bone remodelling. Curr. Opin. Pharmacol. 28, 24–30.
Ramezanzadehkoldeh, M., Skallerud, B., 2017. Nanoindentation response of cortical bone: dependency of subsurface voids. Biomech. Model. Mechanobiol. 16, 1599–1612.
Rodriguez-Florez, N., Oyen, M.L., Shefelbine, S.J., 2014. Age-related changes in mouse bone permeability. J. Biomech. 47, 1110–1116.
Rodriguez-Florez, N., Oyen, M.L., Shefelbine, S.J., 2013. Multi-scale permeability of murine bone measured by nanoindentation. In: Poromechanics V: Proceedings of the Fifth Biot Conference on Poromechanics, pp. 1145–1151.
Shefelbine, S.J., Carter, D.R., 2004. Mechanobiological predictions of growth front morphology in developmental hip dysplasia. J. Orthop. Res. 22, 346–352.
Smit, T.H., Huyghe, J.M., Cowin, S.C., 2002. Estimation of the poroelastic parameters of cortical bone. J. Biomech. 35, 829–835.
Srinivasan, S., Ausk, B.J., Prasad, J., Threet, D., Bain, S.D., Richardson, T.S., Gross, T.S., 2010. Rescuing loading induced bone formation at senescence. PLoS Comput. Biol. 6, e1000924.
Srinivasan, S., Weimer, D.A., Agans, S.C., Bain, S.D., Gross, T.S., 2002. Low-magnitude mechanical loading becomes osteogenic when rest is inserted between each load cycle. J. Bone Miner. Res. 17, 1613–1620.
Tan, S.D., de Vries, T.J., Kuijpers-Jagtman, A.M., Semeins, C.M., Everts, V., Klein-Nulend, J., 2007. Osteocytes subjected to fluid flow inhibit osteoclast formation and bone resorption. Bone 41, 745–751. https://doi.org/10.1016/j.bone.2007.07.019.
Taylor, W., Warner, M., Clift, S., 2003. Finite element prediction of endosteal and periosteal bone remodelling in the Turkey ulna: effect of remodelling signal and dead-zone definition. Proc. Inst. Mech. Eng. [H] 217, 349–356.
Tiwari, A.K., Kumar, R., Tripathi, D., Badhyal, S., 2018. In silico modeling of bone adaptation to rest-inserted loading: strain energy density versus fluid flow as stimulus. J. Theor. Biol. 446, 110–127.
Tiwari, A.K., Prasad, J., 2016. Computer modelling of bone's adaptation: the role of normal strain, shear strain and fluid flow. Biomech. Model. Mechanobiol. 1–16. https://doi.org/10.1007/s10237-016-0824-z.
Van Rietbergen, B., Huiskes, R., Weinans, H., Sumner, D., Turner, T., Galante, J., 1993. The mechanism of bone remodeling and resorption around press-fitted THA stems. J. Biomech. 26, 369–382.
Wang, L., 2018. Solute transport in the bone lacunar-canalicular system (LCS). Curr. Osteoporos. Rep. 16, 32–41.
Weinbaum, S., Cowin, S., Zeng, Y., 1994. A model for the excitation of osteocytes by mechanical loading-induced bone fluid shear stresses. J. Biomech. 27, 339–360.
Wolff, J., 1893. Das gesetz der transformation der knochen. DMW-Dtsch. Med. Wochenschr. 19, 1222–1224.